# FURTHER STUDIES AND EXPERIMENTAL RESULTS ON BOUNDARY GUIDED TRAVELING-WAVE PARTICLE HANDLING

Felix M.Moesner[1,2], Toshiro Higuchi[2,3], Manfred H.Hertwig[4], and Yoshikazu Tanii[2,5]

[1] *Swiss Federal Institute of Technology Zurich • Institute for Robotics (IfR)*
*ETH Center / CLA, 8092 Zurich, Switzerland • Fax: +41 1 632 1078 • Email: moesner@ifr.mavt.ethz.ch*

[2] *Kanagawa Academy of Science and Technology • Higuchi 'Ultimate Mechatronics' Project*
*KSP Bldg., East 405, 3-2-1 Sakado, Takatsu-ku, Kawasaki 213, Japan • Fax: +81 44 819 2095*

[3] *University of Tokyo • Department of Precision Machinery Engineering*
*Hongo 7-3-1, Bunkyo, Tokyo 113, Japan • Fax: +81 3 5800 6968*

[4] *Swiss Federal Institute of Technology Zurich • Institute of Design and Construction Methods (IKB)*
*ETH Center / CLA, 8092 Zurich, Switzerland • Fax: +41 1 632 1181*

[5] *Pure Material Laboratory Ldt.*
*5-30-1 Kumegawa-cho, Higashimurayama City, Tokyo 189, Japan • Fax: +81 423 94 4500*

## ABSTRACT

Different small-scale devices for particle micro-handling using an AC electric field boundary wave were proposed in an earlier paper of the authors[1]. These devices, with various novel transportation and manipulation features, that instantly generate particle driving forces through electric field creation, have been designed and produced. In a further endeavor, the mechanisms of particle conveyance are here subsequently validated in experiments.

Particles on a thin protecting and insulating film interface above a series of encased and insulated parallel field electrodes become either tribo-electrically or induction charged through the application of balanced three- or six-phase voltages. The created non-uniform traveling field-wave conveys the charged particles perpendicular to the electrodes by repulsive forces in a hopping mode from electrode to electrode.

In a temperature and humidity controlled environment, experiments surveying particle conveyance dynamics on these electric devices have been carried out. Various particle materials with diameters up to 400 µm have been examined; metal, glass, and plastic spheres showed the best performances. The transient charge distribution on particles and on the activated electric device, which is responsible for the particle conveyance, has been statically and dynamically inspected by a modified scanning electron microscope. Theoretical considerations underline the experimental findings. Further, angular speckle contouring measurements reveal the manipulation surface profile. Finally, a selection of cover materials are examined for their particle conveyance qualities.

**Keywords:** particle, micro-handling, electric field, potential distribution, angular speckle contouring, cover material

## 1. INTRODUCTION

In modern industry, there are several implemented techniques employed for particle handling. Each technique is suited to a particular goal in the process and also may take advantage of a specific particle property. These handling methods include classical air- and fluidborne transportation by regulated carrier gas or liquid flow. Particles are conveyed in bulk in long flexible tubes and pipes[2]. This purpose-oriented guidance of a mass of particles to a fixed target container, render micro-manipulation of single objects nearly impossible. Similarly, transportation by surface vibrations carries a bulk of particles to a fixed spot. Apparati incorporating this technique form the group of parts feeder which was conceived purely for mass transportation and not for the controlled micro-manipulation of objects.

In some cases, an explicit particle-property is set as conveyance trigger. This is demonstrated by the usage of magnetic fields to manipulate fine magnetic particles[3,4]. High gradient magnetic separation enables even the effective han-

SPIE's International Symposium on Intelligent Systems and Advanced Manufacturing
Proceedings on Microrobotics: Components and Applications, Boston, USA, November 1996, vol. 2906, pp. 118 - 127.

dling of very weakly magnetic particles of micron size[5]. The advantage lies in the property-oriented separation of particles into two different groups of magnetic and non-magnetic objects. However, this technique prevents the handling of purely non-magnetic particles.

In contrary to above methods, it is conceivable to use tiny grippers or shovels for single particle manipulation. The goal of these systems is to handle and assemble micro structures. A solution is the grasping and holding of small particles or cells by using microgrippers[6]. Further, a nanorobotic system which was assigned the task of automated handling of micro-parts with nanometer resolution has been developed[7]. This goal-oriented method allows manipulation of single particles despite their different properties.

Listed methods are related by the common application of particle handling. However, they are all together restricted to a particular range of handling abilities, such as bulk transportation, single handling or property-oriented manipulation. With the appropriate use of *electrostatic* forces however, it is possible to create very compact devices for particle handling, possessing advantages over the above mentioned methods and therefore providing an interesting alternative.

The method of using electrostatic forces for particle handling has already been outlined in various papers and proven in applications. DC electrostatic forces were engaged in surface cleaning and particle dispenser processes[8]. Transportation of fine particles by a three-phase traveling electric field was originally proposed Masuda in the early seventies[9]. The discovery has been reported as an *electric curtain*, where aerosol particles are continuously levitated against gravity. Frequency and phase-lag effects on fine particle transportation for the electric curtain mode have been theoretically studied[10], where systems with wide electrode gaps have been proposed. Linear motion of microscopic objects and manipulation of cells are presented in other papers[11, 12].

This paper focuses on devices for particle transportation and manipulation in the interface between the micro- and macro-world by making use of AC electric fields as the contactless particle conveyor. By this technique, a range of heterogeneous particle substances showed an effective frequency dependent transportation performance. The devices are connected to and activated by a multi-phase, programmable, high voltage supply with a profile amplitude range of up to 2 kV. The energizer electrodes integrated into the devices are situated at equal distance to each other and possess different designs, such as parallel or dot-shaped conductors forming the *electric panel* and *electric dots* devices.

Since no moving machine parts are involved, the forces of the electric field can reduce overall energy consumption. It is expected that the described approaches will lead to new applications in various fields, such as a parts feeder and manipulator for micro electro mechanical systems.

## 2. Principle of Conveyance

To explain the traveling wave principle, only slim and long parallel electrodes with a constant gap, which form the skeleton of the *electric panel*, shall be considered in the following interpretation.

Balanced, multi-phase high voltages from a programmable source are supplied to a series of encased, parallel electrodes which are covered and protected against electrical breakdown by a thin insulating film. Upon the activation of the electrodes, a traveling electric field is created around the electrodes which is transiently changing in sync with the applied voltage phase.

Particles on the thin insulating film interface above the encased and insulated parallel field electrodes become, depending upon the material, either triboelectrically or induction charged through the application of voltages to the electrodes. Dynamic forces from the created non-uniform traveling field-wave overcome the adhesion and gravitational forces of the charged particles and convey them in a direction in the plane perpendicular to the electrodes in a hopping mode from electrode to electrode.

A multi-channel, programmable, high voltage supply is attached to the electric device, where every sixth electrode belongs to the same phase state: *a*, *b*, *c*, *d*, *e*, or *f*. Fig. 1 shows the principle of the electrode connection to each phase.

The supply sequence from the voltage source to the electrodes is given in Table I. Considering balanced square profile voltages, for a better understanding, the sequence is written with [+], [0], and [-] for a three- and a six-phase supply representing the 3 voltage states. The six-phase case requires all of the 6 attachments, whereas in the three-phase case, *a* and *d*, *b* and *e*, *c* and *f* are connected to the same phase. Particle transportation occurs with the variation of the sequence, i.e. the particle synchronously moves with one phase. As a consequence, within one six-phase period, the particle is conveyed along a distance double that of one three-phase period.

Particles involved in the experiments were in the 5 µm to 400 µm diameter range. Various metals, glass, and plastic spherical particles gave the best results in a series of conveyance tests. A selection of 70 different types of substances have been examined, and about half of the tested particle materials showed an acceptable frequency-dependent transportation behavior. Raising the frequency above the 100 to 200 Hz range, caused the particle movement to cease with our employed devices. It has been observed that spherical particles smaller in diameter than the pitch-length were suitable for conveyance in most of the experiments. For the following experiments, we focused on the usage of spherical, metal and glass particles. Representative samples are shown on the right side in Fig. 2.

## 3. Electric Panel Devices: Fabrication

As shown in the cross-sectional view of Fig. 3, the *electric panel* device is composed of parallel electrodes encased in epoxy resin, an insulating thin cover-film, a supporting panel, and electrode-attachments to the phases of the power supply. It is important to guarantee sufficient insulation between the electrodes which can resist an electric field strength of 57 kV/cm or more.

The parallel electrodes of the *electric panel* have an average center-to-center pitch length of 400 µm, a diameter of 50 µm and are situated parallel to the surface at a distance of 25 µm to 75 µm. Compared to other proposed devices, the *electric panel* represents the most compliant device. Due to the simple electrode design, more flexibility can be added to the device by increasing the number of connectable voltage phases. Six is directly dividable by two and three, so it is conceivable to use one and the same device with a six-phase attachment in a two- or three-phase mode.

Fig. 4 shows the perspective view of an *electric panel* for bi-directional particle transportation. The particles are conveyed rectangular to the electrodes in one direction across the entire surface and by reversing the voltage supply sequence, the particles are transported in the other direction.

An approach to achieving multi-directional particle handling is shown in Fig. 5. A second electrode layer perpendicular to the first can be added with a sufficient insulation gap between them. Alternatively, a mesh interweaving the two layers can be employed as shown in Fig. 6 and utilized in the *electric panel* described and employed herein. In order to endure high voltage differences at the nodal points which can be as high as 666 kV/cm, individual mesh-electrodes must be covered with a sufficient insulation such as polyamide-imide. This insulator assures a dielectric strength of up to 2756 kV/cm under ambient conditions. Particles can be conveyed two-dimensionally over the entire surface; this includes tetra-directional motion when the two electrode sets are activated separately. Octal-directional manipulation is reached by the combined energizing of the two sets.

A view of the real *electric panel* is kept as a picture in Fig. 6. The field electrodes possess a voltage supply at one end and remain insulated at the other. By this structure, the electrodes function as capacitors with a capacitance of approximately 260 nF in the employed frequency range. The total particle manipulation surface has dimensions of 100 x 75 mm$^2$. A section of the surface is magnified and represented as a SEM image. It illustrates the mesh structure of the field electrodes. The entire panel is covered by a thin film and hermetically sealed by epoxy resin in order to increase safety during operation.

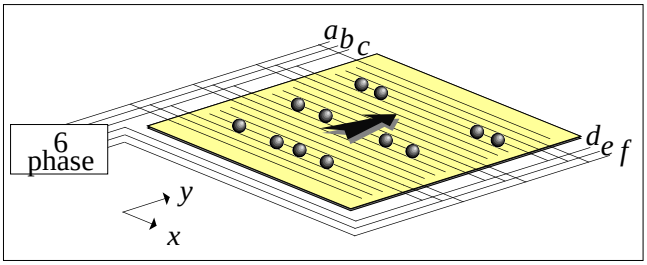


*Fig. 1: Electrode connection to each of the six phases a, b, c, d, e, and f.*

TABLE I

6 Electrode Attachments *a, b, c, d, e,* and *f* and their Supply from a Multi-Phase Voltage Source

Sequence

| *a* | *b* | *c* | *d* | *e* | *f* |
|---|---|---|---|---|---|
| + | - | 0 | + | - | 0 |
| + | 0 | - | + | 0 | - |
| 0 | + | - | 0 | + | - |
| - | + | 0 | - | + | 0 |
| - | 0 | + | - | 0 | + |
| 0 | - | + | 0 | - | + |

Supply sequence of three-phase square profile voltages

| *a* | *b* | *c* | *d* | *e* | *f* |
|---|---|---|---|---|---|
| + | + | 0 | - | - | 0 |
| 0 | + | + | 0 | - | - |
| - | 0 | + | + | 0 | - |
| - | - | 0 | + | + | 0 |
| 0 | - | - | 0 | + | + |
| + | 0 | - | - | 0 | + |

Supply sequence of six-phase square profile voltages

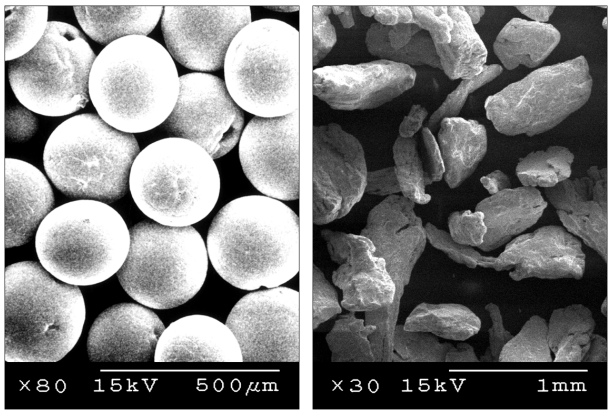


*Fig. 2: A SEM micrograph of representative spherical and rugged iron particles.*

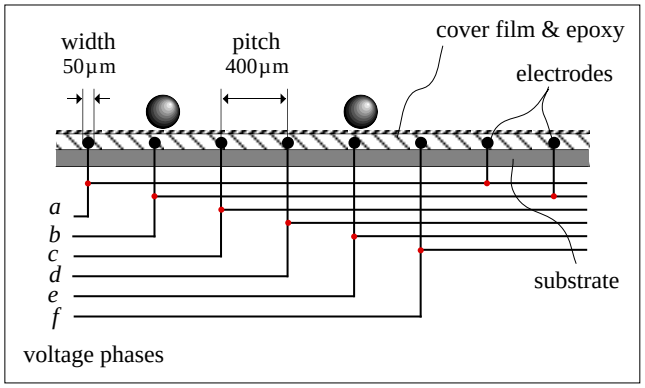


*Fig. 3: Cross-section of the electric panel revealing its structural composition. Every sixth electrode is attached to the same phase.*

## 4. Potential Distribution of Electric Fields

In experiments with small particles, panels are employed in various actuation modes such as three- and six-phase. Furthermore, the individual single phase voltage can be of a particular wave profile such as sine, pulse, triangular or other. It is now of interest to obtain the potential distribution of the electric fields over and in an *electric panel*. The focus of the following calculation is the pulsed wave profile.

### *A. Calculation*

Finding the potential distribution in the region between two conductors, given the charge distribution on the surfaces of the conductors or the potentials of the conductors or a combination of the two, is a problem for which Laplace's equation (1) can be used. In our case, we consider the solution of the two-dimensional Laplace equation (2).

$$\nabla^2 V = 0 \tag{1}$$

$$\frac{\partial^2 V}{\partial x^2} + \frac{\partial^2 V}{\partial y^2} = 0 \tag{2}$$

Generally, an equation of this type is solved by the analytical technique, the *separation of variables*. However, it has been considered to employ a numerical solution in order to take advantage of fast computers (Sun Ultra 1 Creator). The method employed is derived from the finite-difference approximation[13]. The *finite-difference method* is the basis for this computer solution.

14 mesh-electrodes of the *electric panel* have been defined in a matrix and connected to their appropriate phase *a*, *b*, *c*, *d*, *e*, and *f*. The matrix is traversed iteratively by means of the finite-difference approximation until the computed error is smaller than a defined constant.

### *B. Results*

The computational calculations of the potential distribution are shown in Figs. 7 and 9 in graphical form. The applied phase-voltage values are listed in Table II.

The result in Fig. 7 refers to the graphical computation of a three-phase case. The graph in Fig. 9 is obtained by a potential distribution calculation of a six-phase voltage supply to the electrodes. In both diagrams, the same three- or six-phase supply sequence has been chosen for the other activation dimension. As a result, a checker board pattern is obtained. The potential of each electrode has been kept in the range of ±10 V. The white and black areas represent the 10 V and -10 V level respectively. The number of equipotential lines is 9 between the minimum and maximum potential.

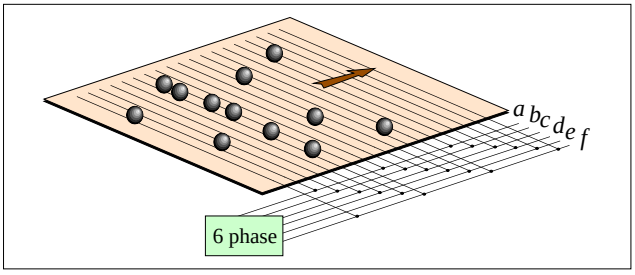


*Fig. 4: Electric panel for bi-directional particle transportation perpendicular to the electrodes.*

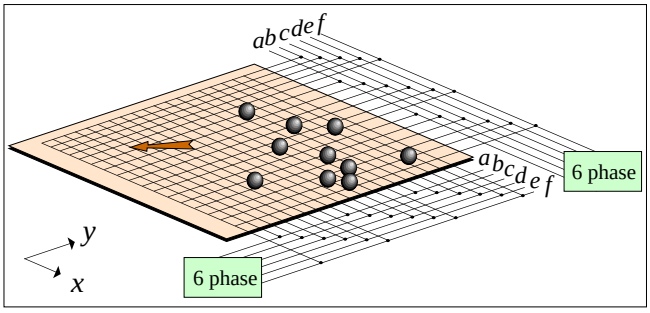


*Fig. 5: Electric panel for tetra- and octal-directional particle handling. Highly insulated electrodes are woven to a mesh.*

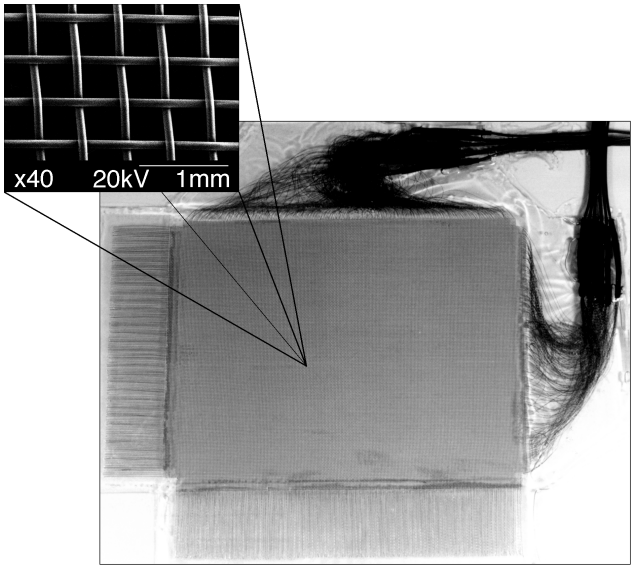


*Fig. 6: Electric panel with magnified mesh-structure of the electrodes.*

TABLE II

PHASE VOLTAGES USED IN POTENTIAL DISTRIBUTION CALCULATIONS.

| three-phase | six-phase voltages | |
|---|---|---|
| *a* = 0 V | *a* = -10 V | *b* = 0 V |
| *b* = -10 V | *c* = 10 V | *d* = 10 V |
| *c* = 10 V | *e* = 0 V | *f* = -10 V |

The two SEM micrographs of Fig. 8 depict the charge distribution on an activated *electric panel*. The SEM works as a charge distribution sensor and has therefore been modified to hold our experimental device. The white parts in the image represent the negative charge on the surface. Positive charge is not detected by the SEM and therefore appears black. Since charge and potential is considered to be analogous, the SEM images can be compared directly with the potential distribution calculation of Figs. 7 and 9. White frames have been shown to visualize a place where the SEM images fit into. It is not difficult to apprehend a good agreement with the overall pattern-structure.

A clear difference between the white areas of Figs. 7 and 9 is the size. The energizing pattern of three-phase voltages produces small, but more numerous activation areas as compared to the six-phase pattern where the activation areas are approximately 4 times larger, but also 4 times fewer in number on the same sized surface. This circumstance reflects the observation of different particle conveyance mannerisms for the three- and six-phase case. It has been noted that a larger activation area is responsible for transportation of larger particles than a smaller area. On the contrary, it appears that smaller activation areas allow more sophisticated handling of particles.

The potential distribution calculation in Fig. 9 corresponds very well with the checker board pattern of conveyed particles in Fig. 10. The white frame visualizes the location which the computed graphic of Fig. 9 matches. The photograph does not disclose particles which are positively or negatively charged. They are simply attracted to the black and white activated areas of Fig. 10. One activated node area is shown by a SEM image in Fig. 11; it is very clear to comprehend that the particles are attracted to and concentrated in an energized spot.

## 5. Observation of Particle Conveyance

The usage of a modified SEM opens many possibilities not only for the static observation of charge distribution on activated electric devices, but leads to the dynamic observation of traveling charge distribution and particle conveyance. For this purpose, a few particles have been positioned on the manipulation surface.

The motion was captured in the TV mode of the SEM. The sequence in Fig. 12 is the result of a single particle following the traveling field wave of a six-phase supply. It should be noted, that the particle uses the *tracked conveyance technique,* which is described in detail in an earlier paper[1]. Specifically, the track holds the particle on a line, which is visible as a static charge distribution in the recorded sequence of Fig. 12. The perpendicular electrodes actuate the particle. The sequence reveals how the particle moves step by

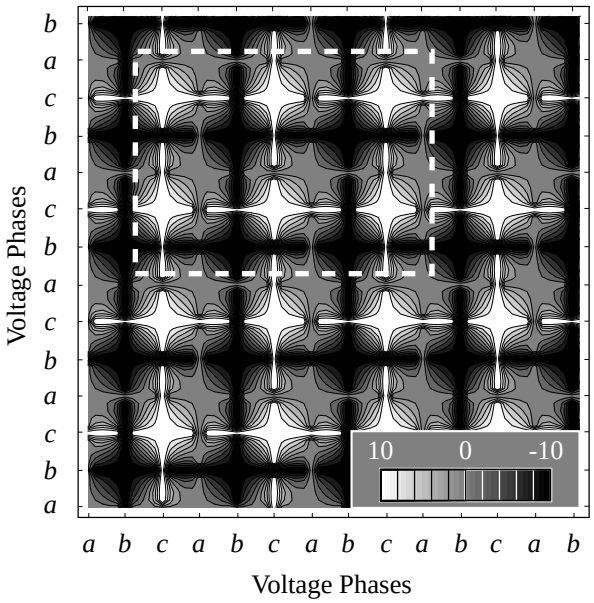


*Fig. 7: Potential field calculation of an electric panel with three-phase voltage supply.*

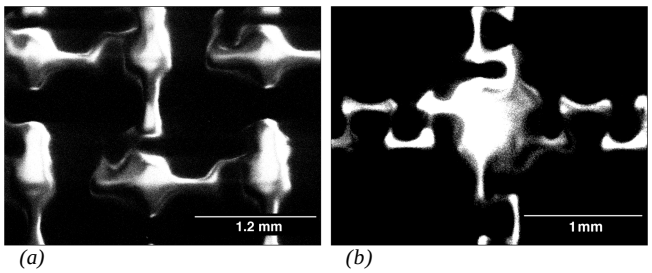


*Fig. 8: SEM micrographs of an activated electric panel. The left segment is three-phase, the right is supplied by six-phase voltages.*

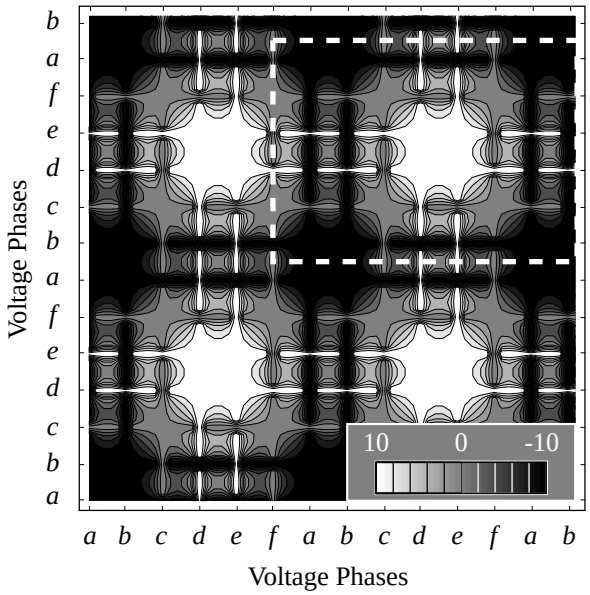


*Fig. 9: Potential field calculation of an electric panel with six-phase voltage supply.*

step over a length of 6 electrode-pitches. The distance is about 2.0 mm. This sequence from (a) to (f) illustrates two facts: first, the particle is conveyed by the electric field of the AC activated electrodes and second, the particle is kept on a line by the DC energized electrodes.

## 6. Electric Dots Device

### *A. Fabrication*

The *electric dots* and *panel* device consist of a very similar structure and are functionally closely related. The main difference is the shape of the field electrodes. They are designed as long parallel electrodes in the panel, but as pinpoint electrodes in the other device. The effect of the traveling electric field is the same, but the positioning of the particles is more individual and precise with the dot matrix. Fig. 13 illustrates the structure of the dot matrix device. All electrodes are embedded in epoxy resin. Their terminal ends are cut perpendicularly and form, together with the body, the manipulation surface. The individual field electrodes are connected to their corresponding voltage phase. In practice, a sandwich structure of neatly cut *electric panel* layers delivers the desired dot electrodes in a matrix configuration. The SEM photo in Fig. 14 depicts the dot electrodes in the manipulation surface, which are visibly composed like a sandwich. Our realized matrix has a (6 x n)-dimension, i.e. it consists of 6 rows. The two central rows are responsible for particle actuation and the remaining four peripheral rows provide a potential track for the particles through their DC activation. The dots in the SEM picture of Fig. 14 are horizontally activated allowing the wave to travel either from left to right or vise versa.

### *B. Phase Lag*

One effect which has been observed in experiments and theoretically described[10] is the phase-lag between the advancing traveling electric field and the conveyed particle. It has been be noted that the particle still remains at a location while the traveling field wave is proceeding. A dynamic sequence of SEM images is shown in Fig. 15. It exposes the close-up actuation of a group of 100 µm glass particles in the direction of the inserted arrow on the manipulation surface of an *electric dots* device. A three-phase electrode activation has been chosen to pay attention to this effect in more detail.

In (a) and (b), the particles remain on a particular spot while the field travels to the next location; then the particles follow (c) and stay again (d) while the field is proceeding. Finally, they follow on as shown in (e). This effect appears as particles try to find an equilibrium between the transiently changing repulsive and attractive forces of the traveling field-wave.

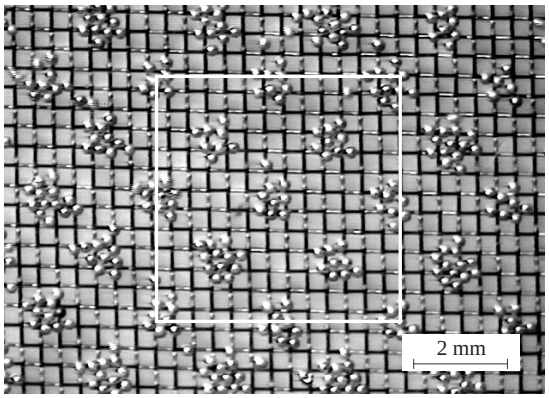


*Fig. 10: Checker board pattern groups of conveyed particles on panel.*

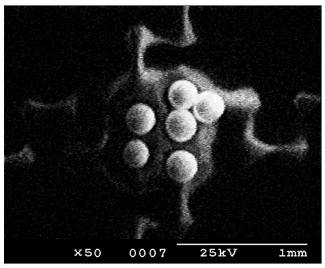


*Fig. 11: SEM image of iron particles attracted to an activated mesh area.*

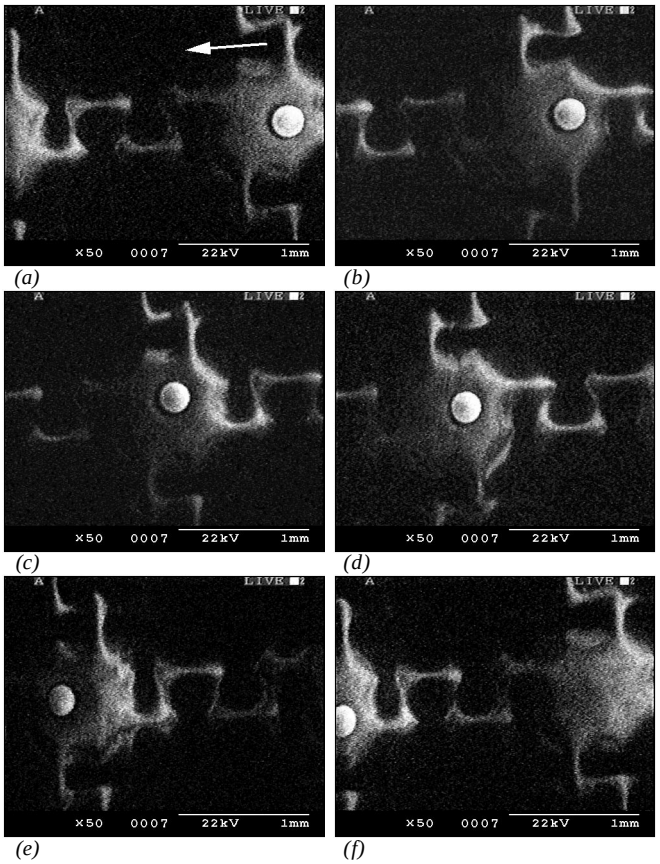


*Fig. 12: Dynamic sequence of SEM images revealing tracked conveyance of a single particle from right (a) to left (f).*

## 7. HOPPING HEIGHT

The dynamic particle conveyance characteristic includes the hopping height as an assigned element when particles move stepwise from electrode to electrode. The following experiment has the aim to examine the hopping height on the *electric panel* device while particles are conveyed towards an film layer verge. Iron particles with an average diameter of 250 µm were employed in this observation. As depicted in Fig. 16, a number of particles are barred by the edge of a film (a); whereas most of the particles were successful in surmounting the fringe in (b) – only a few were left behind. Three variables were taken into account: the thickness of the film layer, the applied voltage amplitude and the frequency. The rim of the film layer is positioned exactly between two electrodes. It is the location of expected maximal hopping height of an actuated particle. It is believed that the repulsive force is accountable for the major part in this hopping nature.

Several experiments were carried out at the ambient atmospherical condition of 20˚C and 30% RH. The *electric panel* with an electrode pitch of 400 µm has been activated by six-phase pulse voltage profiles as introduced in Table I. The averaged results are revealed in Fig. 17. The first graph (a) depicts the rate of successful particles overcoming the film fringe of 5 µm. At a low voltage of 100 V amplitude, the frequency of approx. 13 Hz shows the highest rate, which is easily increased by raising the applied voltage. The phase voltage of 250 V amplitude shows a rate of even more than 95 % above 5 Hz which indicates that many particles jump even higher than 5 µm. The hopping height diminishes in relation to a higher applied frequency. The rate of particles overcoming the 25 µm edge is represented in (b) – here, the frequency-dependent hopping height can be easily seen. Increasing the applied voltage allows particles to hop over a fringe height of 50 µm (c) and even 100 µm (d). A height reduction by an increased frequency could hardly be conceived within the examined range.

## 8. TOPOGRAPHY OF MANIPULATION SURFACE

Angular Speckle Contouring (ASC) measurements[16] are used to develop a qualitative picture about the condition of the surface boundary, where particles are actuated on. This non-contacting, optical full-field measurement technique using speckle interferometry enables reproduction of topographical surface information. Through a beamsplitter, resultant optical path difference images are captured in a CCD camera and algorithms reconstruct the 3D geometrical structure of the surface[17].

This method is applied to the surfaces of two *electric panel* devices of mesh type and the results may be seen in Fig. 18 as the 3D surface topography of an early version (left) and a second, improved version (right). The scanned

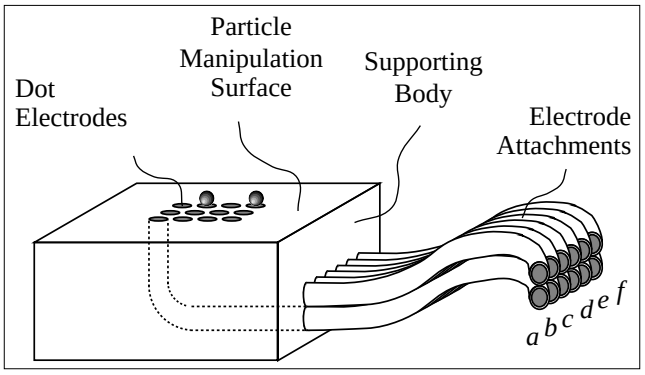


*Fig. 13: Perspective of the* electric dots *device. The field electrodes are embedded in a epoxy resin body and connected to their phases.*

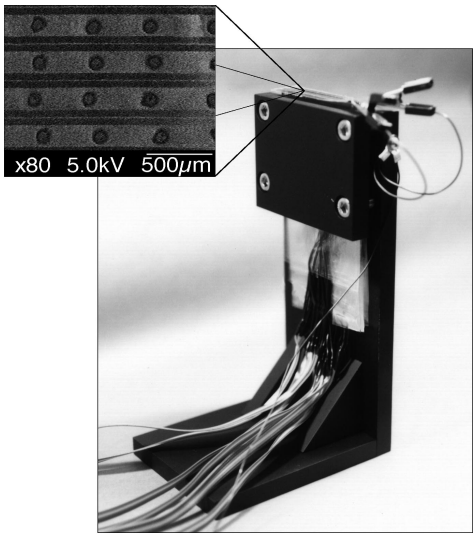


*Fig. 14: Experimental setup of the electric dots device. The handling surface is at the top and magnified by a SEM image revealing its matrix dot electrodes in a sandwich structure.*

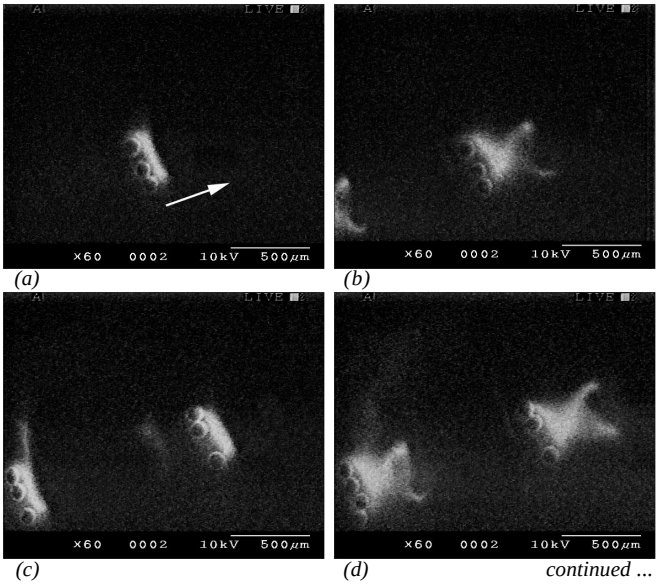


*(a)* *(b)* *(c)* *(d)*

*continued ...*

surface measures 9.7 x 6.8 $mm^2$. The earlier version is constructed bottom-up without vacuum molding method while the improved version is built top-down with vacuum molding. Although the overall peak-valley which represents the difference between minimum and maximum profile value is determined as root-mean-square (RMS) to 22.63 µm and to 11.19 µm for the first and second examination, respectively. Fig. 18 fails to make clear the difference in character of both surfaces. For this reason, the profile along a line in *y*-direction is evaluated for both cases and represented in Fig. 19 revealing a clear difference in valley depth. The hollows are drastically improved in the second sample.

In an attempt to analyze the distribution of valley depth over the surface, profiles such as in Fig. 19 are evaluated along the complete length of the *x*-axis, and the peak-valley for each profile is obtained. Thus, the distribution of all peak-valleys along the *x*-axis is represented for the first and second, improved sample (Fig. 20). As a result, it is to note, that the improved sample has hollows of nearly the same width, but with valley depths reduced by a factor of two and more. Flatter, more even surface topography directly benefits the conveyance quality of particles, especially in the care of very fine particles which could easily become trapped in crevices.

## 9. Surface Cover Material

The material of the cover film influences the particle actuation. It has an essential impact of the particle charging capability and the penetration of the electric field through the layer. Generally, the relaxation time of the charge on the cover surface is dependent on the permittivity and conductivity of the material.

In an attempt to characterize some cover materials, the quality of particle actuation is observed at various supplied voltages and frequencies. It is assumed that the result has a direct correlation with the examined cover material.

The experimental setup consists merely of the *electric panel* device, the pulse voltage supply, and the observing microscope. At an ambient condition of 22° C and 31% RH, particles are placed on the manipulation surface under the objective lens. Iron particles of the sort used in previous experiments are taken as the experimental specimen.

A selection of distinct cover materials is employed in a test sequence that include: a 85 µm thick plain paper copy (PPC) sheet (Light Printing PPC, Kyoyoushi Corp., Japan), a 95 µm PPC paper sheet (Xerox Paper, Fuji Xerox Co. Ldt., Japan), a 100 µm overhead projector (OHP) transparency film (PPC transparency film, Sumitomo 3M Ldt., Japan), a 127 µm OHP transparency film (OHP sheet, Seiko Epson Corp., Japan), a 10 µm cellophane film (New Kurerapp, Kureha Chemical Ind. Corp., Japan), and a 145 µm

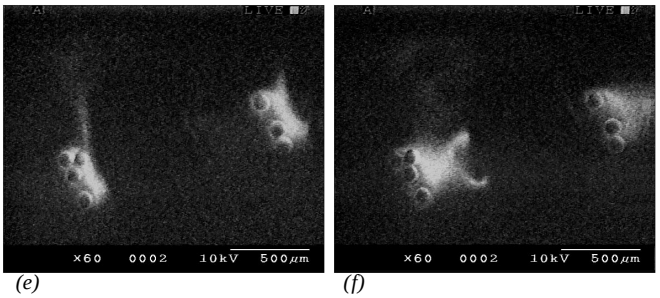


*(e)* *(f)*

*Fig. 15: Dynamic sequence of SEM images revealing the actual phase-lag between traveling field and conveyed particle. The glass particles show an actuation in direction of the arrow.*

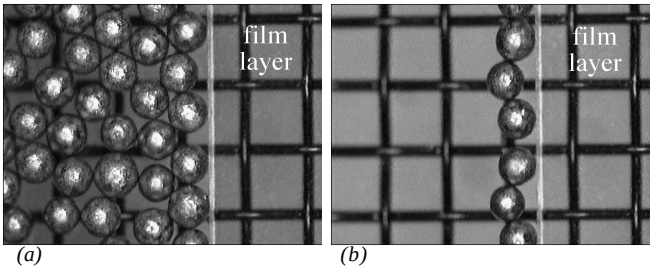


*(a)* *(b)*

*Fig. 16: Experiment used for observation of particle hopping height during conveyance. Film layer fringe in (a) stops most of the test particles, whereas in (b) only few are left.*

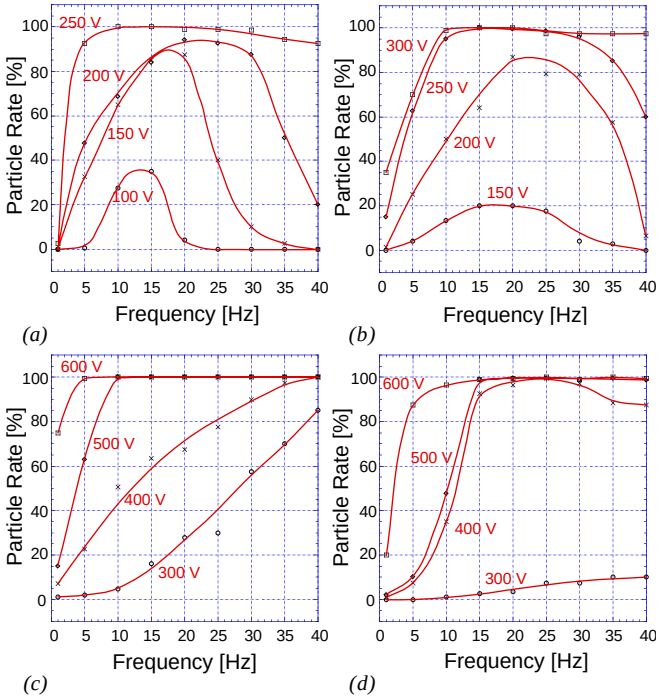


*(a)* *(b)* *(c)* *(d)*

*Fig. 17: Graph of successful particles versus frequency at various excitation voltages. Film layer heights: (a) at 5 µm , (b) at 25 µm, (c) at 50 µm and (d) at 100 µm.*

glass sheet (Micro Cover Glass, Matsunami Glass Ind. Ltd., Japan).

A broad, thin cover sample is affixed neatly onto the manipulation surface. Particulate samples on the cover film are tested and observed at a supplied voltage amplitude range between 150 V and 600 V. The frequency of the employed six-phase supply is swept from 1 Hz to 40 Hz. The quality of the particle actuation is determined by estimation of the quantitative number of conveyable particles. Hence, the quality is classified into four levels ranging from no actuation to excellent particle actuation. The characteristic is presented in the following graphs with a shading which varies between dark and light representing poor and good particle motion, respectively. The discrete experimental data has been fitted and smoothed in order to obtain these characteristic curves.

Figs. 21 and 22 depict each the particle actuation quality of PPC paper sheets. The characteristic reflects a clear dependence on the applied voltage level and frequency. The response of both samples improves with a higher voltage amplitude. The optimal frequency range is cover-material-dependent at around 15 Hz for the first and 10 Hz for the second sample. Since the PPC paper sheet is especially produced for xerography, the paper incorporates an electrostatic affinity that enhances the copy quality. This property of the cover material negatively affects good actuation of particles, however. Furthermore, paper is a moisture-absorbent, hydrophilic material which also hampers electric field penetration to a degree.

The characteristics of the OHP transparency film are presented in Figs. 23 and 24. Similar to the previous two samples, the cover material of Fig. 23 is designed for PPC usage and shows therefore an analogous characteristic with the exception of a higher frequency acceptance. The material sample in Fig. 24 is originally designed for inkjet printers. Since this film is free of special electrostatic affinity coatings, an excellent particle actuation is reached for higher voltage amplitudes at a frequency of around 10 Hz. Films tend to accumulate moisture on the surface, rather than absorbing it interiorly. It is assumed that this improves electric field penetration.

Figs. 25 and 26 describe the results of two materials with very dissimilar thicknesses. The cover material in Fig. 25 is a very thin cellophane film with a similar behavior to the OHP transparency films. It permits an acceptable particle actuation over a wide voltage amplitude and frequency range. Good characteristics start at a higher voltage at around 17 Hz. The conveyance qualities of the glass sheet in Fig. 26 increase with voltage. Best particle actuation is obtained at around 13 Hz. In spite of the greater thickness, glass as a material adds a good dynamic charge accumulation property to the surface.

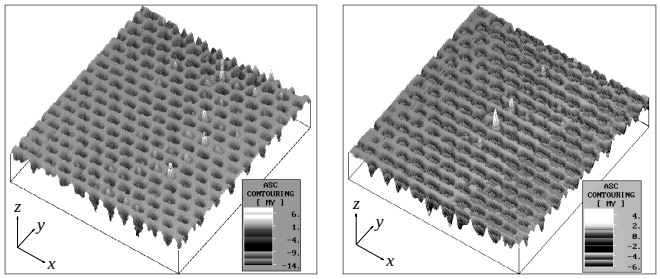

*Fig. 18: Topography of electric panel devices: early type (left) and improved type (right)[17].*

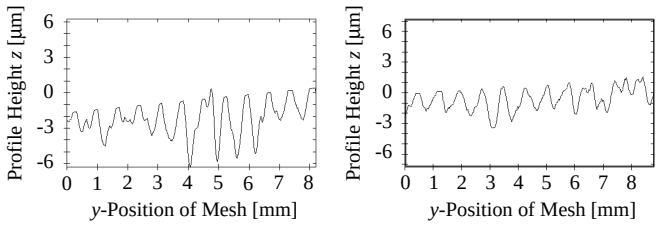


*Fig. 19: Profile evaluation along a line in y-direction reproduced for both panel samples[17].*

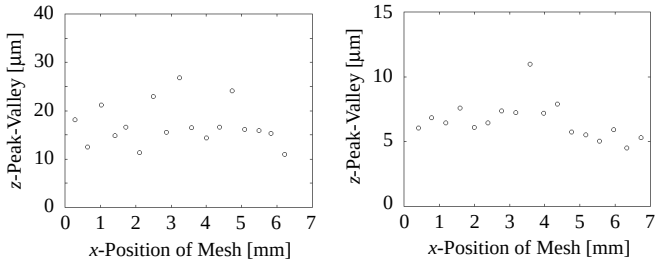


*Fig. 20: Global comparison of the peak-valley values determined line-by-line, again for both panel samples[17].*

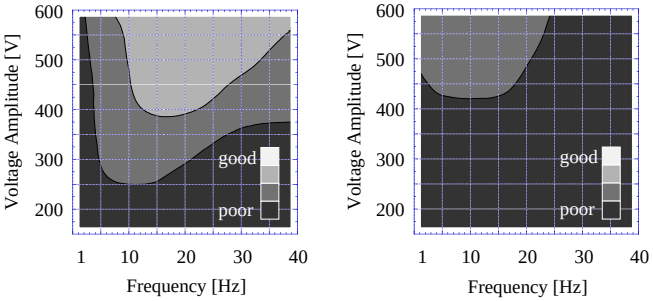


*Fig. 21: Particle actuation characteristic on 85 µm thin PPC paper sheet (Kyoyoushi Corp. sample).*




*Fig. 22: Particle actuation characteristic on 95 µm PPC paper sheet (Fuji Xerox Co. Ldt. sample).*

The results of this experimental series concludes the affirmative utilization of some cover materials for particle actuation. Further, hydrophilic PPC paper sheets with their natural affinity for moisture prevent ultra-high resistance in ambient conditions which leads to weak particle actuation. The remaining cover materials yield overall good particle actuation characteristics. The potential usage of glass as a cover material is undoubtedly a boon to many applications.

## CONCLUSION

The potential distribution of electric fields in a three- and six-phase mode has been calculated and validated with charge distribution SEM images. Both results show very good agreement. The particle conveyance mechanism has been further explained by two SEM image sequences where the phase-lag between traveling wave and particle is commented. As part of the dynamic conveyance characteristic, the particle hopping height is observed and discussed. Further, angular speckle contouring measurements show the difference of manipulation surface profiles. Finally, a selection of cover materials are examined for their particle conveyance qualities among which glass as cover material possesses an interesting performance.

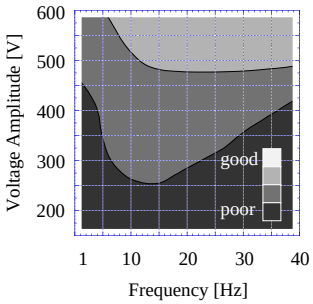


*Fig. 23: Particle actuation characteristic on 100 µm OHP transparency film (Sumitomo 3M Ldt. sample).*

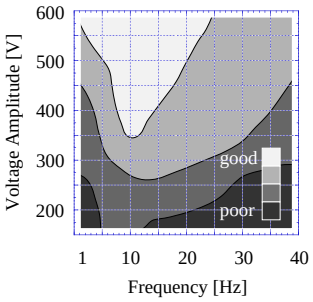


*Fig. 24: Particle actuation characteristic on 127 µm OHP transparency film (Seiko Epson Corp. sample).*

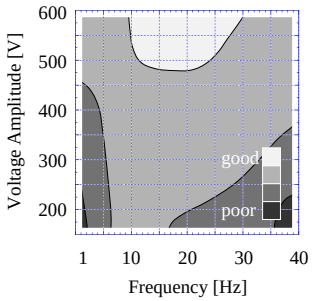


*Fig. 25: Particle actuation characteristic on 10 µm cellophane film (Kureha Chemical Ind. Corp. sample).*

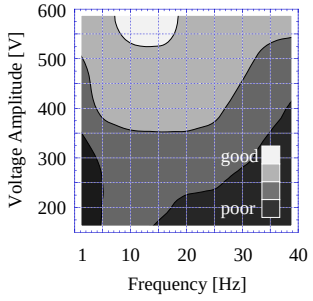


*Fig. 26: Particle actuation characteristic on 145 µm glass sheet (Matsunami Glass Ind. Ltd. sample).*

## ACKNOWLEDGMENT

We wish to acknowledge the appreciated and valuable collaboration of our colleagues S. Yashiro for his engagement in the *electric panel* devices, S. Egawa and T. Niino for their expertise on voltage supply systems, J. Jin and S.J. Woo for prolific discussions, and W. Yang for his contributory involvement in this project.

## REFERENCES

[1] **Moesner**, F.M., and **Higuchi**, T., "Electrostatic Devices for Particle Micro-Handling," *IEEE Industry Applications Society*, 30th Annual Meeting, Orlando, vol. 2, 10 October, 1995, pp. 1302-1309.

[2] **Masuda**, H., **Komatsu**, T., and **Iinoya**, K., "The Static Electrification of Particles in Gas-Solids Pipe Flow," *AlChE Journal*, vol. 22, no. 3, May 1976, pp. 558-564.

[3] **Alward**, U., and **Imaino**, W., "Magnetic Forces on Monocomponent Toner," *IEEE Trans. Mag.*, vol. MAG-22, 1986, pp. 128-134.

[4] **Jones**, T.B., **Whittaker**, G.L., and **Sulenski**, T.J., "Mechanics of Magnetic Powders," *Powder Technol.*, vol. 49, 1987, pp. 149-164.

[5] **Oberteuffer**, J.A., "Magnetic Separation: A Review of Principles, Devices, and Applications," *IEEE Trans. Mag.*, vol. MAG-10, 1974, pp. 223-238.

[6] **Greitmann**, G., and **Buser**, R.A., "Tactile Microgripper for Automated Handling of Microparts," *Sensors & Actuators: A. Physical*, vol. SNA 053 / 1-4, 1996, pp. 409-414.

[7] **Codourey**, A., **Zesch**, W., **Büchi**, R, and **Siegwart**, R., "A Robot for Automated Handling in Micro-World," *IROS'95 IEEE/RSJ*, Pittsburgh, Pennsylvania, August 1995.

[8] **Cooper**, D.W., **Wolfe**, H.L., **Yeh**, J.T., and **Miller**, R.J., "Surface Cleaning by Electrostatic Removal of Particles," *Aerosol Science and Technology*, vol. 13, 1990, pp. 116-123.

[9] **Masuda**, S., **Fujibayashi**, K., **Ishida**, K., and **Inaba**, H., "Confinement and Transportation of Charged Aerosol Clouds via Electric Curtain," *Electrical Engineering in Japan*, vol. 92, no. 1, 1972, pp. 43.

[10] **Gan-Mor**, and S., **Law**, S.E., "Frequency and Phase-Lag Effects on Transportation of Particulates by an AC Electric Field," *IEEE Transactions on Industrial Applications*, vol. 28, no. 2, March 1992, pp. 317-323.

[11] **Fuhr**, G., **Hagedorn**, R., and **Müller**, T., "Linear Motion of Dielectric Particles and Living Cells in Microfabricated Structures induced by Traveling Electric Fields," *Proc. IEEE Micro Electro Mechanical Systems Workshop*, Nara, Japan, January / February 1991, pp. 259-264.

[12] **Pethig**, R., "Applications of AC Electrical Fields to the Manipulation and Characterisation of Cells," *Conference Record 4th Toyota Conference*, October 1990.

[13] **Rao**, N.N., "Elements of Engineering Electromagnetics," *Prentice-Hall Inc. Fourth Edition*, 1994.

[16] **Hertwig**, M.H., **Floureux**, T., and **Flemming**, T., "Applications of Recently Improved Electronic Speckle Pattern Interferometry by Addition of Incremental Images," *SPIE*, vol. 2340, 1994, pp. 124-133.

[17] **Hertwig**, M.H., "Entwicklung neuer speckle-interferometrischer Messmethoden für industrielle Anwendungen," *Dissertation at Swiss Federal Institute of Technology Zurich*, 1997, to be published.